Title

Voltage cycling process for the electroconversion of biomass-derived polyols

Journal

Proceedings of the National Academy of Sciences of the United States of America, 118(41)

ISSN

0027-8424

Authors

Kim, Dohyung

Zhou, Chengshuang

Zhang, Miao

et al.

Publication Date

2021-10-12

DOI

10.1073/pnas.2113382118

Voltage Cycling Process for the Electroconversion of Biomass-derived Polyols

Dohyung Kim[1], Chengshuang Zhou[1], Miao Zhang[2], and Matteo Cargnello[1,3,*]

[1]*Department of Chemical Engineering, Stanford University, Stanford, CA 94305*

[2]*Chemical Sciences Division, Lawrence Berkeley National Laboratory, Berkeley, CA 94720*

[3]*SUNCAT Center for Interface Science and Catalysis, Stanford University, Stanford, CA 94305*

*Correspondence to: mcargnello@stanford.edu

Abstract

Electrification of chemical reactions is crucial to fundamentally transform our society that is still heavily dependent on fossil resources and unsustainable practices. Besides, electrochemistry-based approaches offer a unique way of catalyzing reactions by the fast and continuous alteration of applied potentials, unlike traditional thermal processes. Here, we show how the continuous cyclic application of electrode potential allows Pt nanoparticles to electro-oxidize biomass-derived polyols with turnover frequency improved by orders of magnitude compared to the usual rates at fixed potential conditions. Moreover, secondary alcohol oxidation is enhanced with a ketoses-to-aldoses ratio increased up to 6-fold. The idea has been translated into the construction of a symmetric single compartment system in a 2-electrode configuration. Its operation via voltage cycling demonstrates high-rate sorbitol electrolysis with the formation of H_2 as a desired co-product at operating voltages below 1.4 V. The devised method presents a potential approach to using renewable electricity to drive chemical processes.

A major element in future sustainable scenarios is electrification. The replacement of the usual carbon-heavy processes with renewable electricity-driven approaches is seen as a way to reduce their carbon footprint and decarbonize our society.[1,2] Therefore, much progress has been made in how electrical energy is produced, stored, and converted.[3] Furthermore, there has been growing interest to electrify the chemical sector responsible for a significant portion of products used worldwide.[4–12] Electrochemistry-based approaches can avoid the use of chemical oxidants and thermochemical treatments that are energy-intensive and unsustainable. Moreover, electrocatalytic routes potentially offer finer control over reaction pathways thanks to its nature of bond activation mediated by electrons at electrode surfaces, in contrast to thermocatalytic methods where temperature indiscriminately disrupts multiple chemical bonds simultaneously in a single molecule.

For electrochemical methods to be useful to drive reactions, high reaction rates must be maintained and product selectivity needs to be controlled. Therefore, efforts have largely focused on the design of catalyst materials, from tuning active site motifs to creating large scale architectures to host active sites.[13,14] Understanding the effects of catalyst structure in thermocatalysis has helped guide catalyst design as well by translating similar strategies into electrocatalysis.[15–17] However, improvements in catalytic activity have been limited in some of the challenging reactions, and alternative ways for their electrification have been developed, such as using redox mediators.[6,9,10,12]

One aspect unique to an electrochemical approach compared to a thermochemical process is the ability to quickly apply and adjust energy to the system, whose response is also

rapid. This is often manifested in the form of electrochemical potential pulses. It allows continuously taking advantage of transient states of the system and its surroundings, unlike traditional approaches under steady-state fixed potential conditions. Potential pulsing has proven useful for the conversion of small molecules, such as CO_2 and formic acid. It has been shown to be advantageous in various ways including regeneration of catalytically active defects, removing poisonous species, and altering reaction pathways.[18–21] In addition, short potential pulses can take advantage of the periodic renewal of the surrounding environment, which has been demonstrated optimal for tuning the selectivity of organic reactions.[22,23] It has also been adopted for electropolymerization reactions producing single-molecular polymeric structures.[24]

Here, we apply the idea of continuous alteration of potentials to electroconversion of biomass-derived polyols. Biomass-derived polyols are naturally abundant resources, such as the six-carbon sorbitol that can be readily obtained from cellulose.[25] Their potential as a platform chemical makes them high-value biomass compounds to be utilized through oxidation to various chemicals.[26–28] By the continuous cycling of potential applied to sorbitol electroconversion, we find Pt nanoparticles to exhibit intrinsic activity improvements and unusual selectivity shifts compared to fixed potential conditions. Turnover frequency is enhanced by an order of magnitude and secondary alcohol oxidation is promoted with a ketoses-to-aldoses ratio increased over 6-fold. Similar improvements are demonstrated with other C_3-C_5 polyols as well. Furthermore, we show that potential cycling relies on the high oxidative activity of non-equilibrated Pt surfaces otherwise difficult to maintain in typical conditions. Such knowledge is translated to an electrolyzer in a 2-electrode configuration via a method called voltage cycling (hereafter, voltage refers to the voltage applied between the electrodes in a 2-electrode configuration whereas term

potential is used to indicate the applied potential in a 3-electrode configuration) demonstrating sorbitol electrolysis and co-production of H_2 at fast output rates with applied voltage below 1.4 V.

Platinum nanoparticles with an average size of 1.8 nm supported on carbon (Pt/C) served as a catalyst (Fig. 1a and Supplementary Fig. 1). Pt/C (40 μg_{Pt}) was loaded onto carbon paper (1 cm^2 geometric area) and used as a working electrode in a typical three-electrode H-cell (Supplementary Fig. 2). With sorbitol present in the electrolyte, a decrease in the hydrogen underpotential deposition current was observed indicating a loss in the available Pt surface area (Supplementary Fig. 3). This is due to the dissociative adsorption of sorbitol on Pt to yield $*CO_{ads}$ as previously described.[29] Multiple potential cycles in between 0.02 to 0.6 V (vs. RHE) avoiding $*CO_{ads}$ oxidation led to a continuous loss of available area, which could only be recovered by positively biasing the electrode to oxidize the $*CO_{ads}$ to CO_2 (Supplementary Fig. 3). Thus, we found that potentials >0.6 V were necessary to convert sorbitol without CO poisoning the surface of Pt nanoparticles.

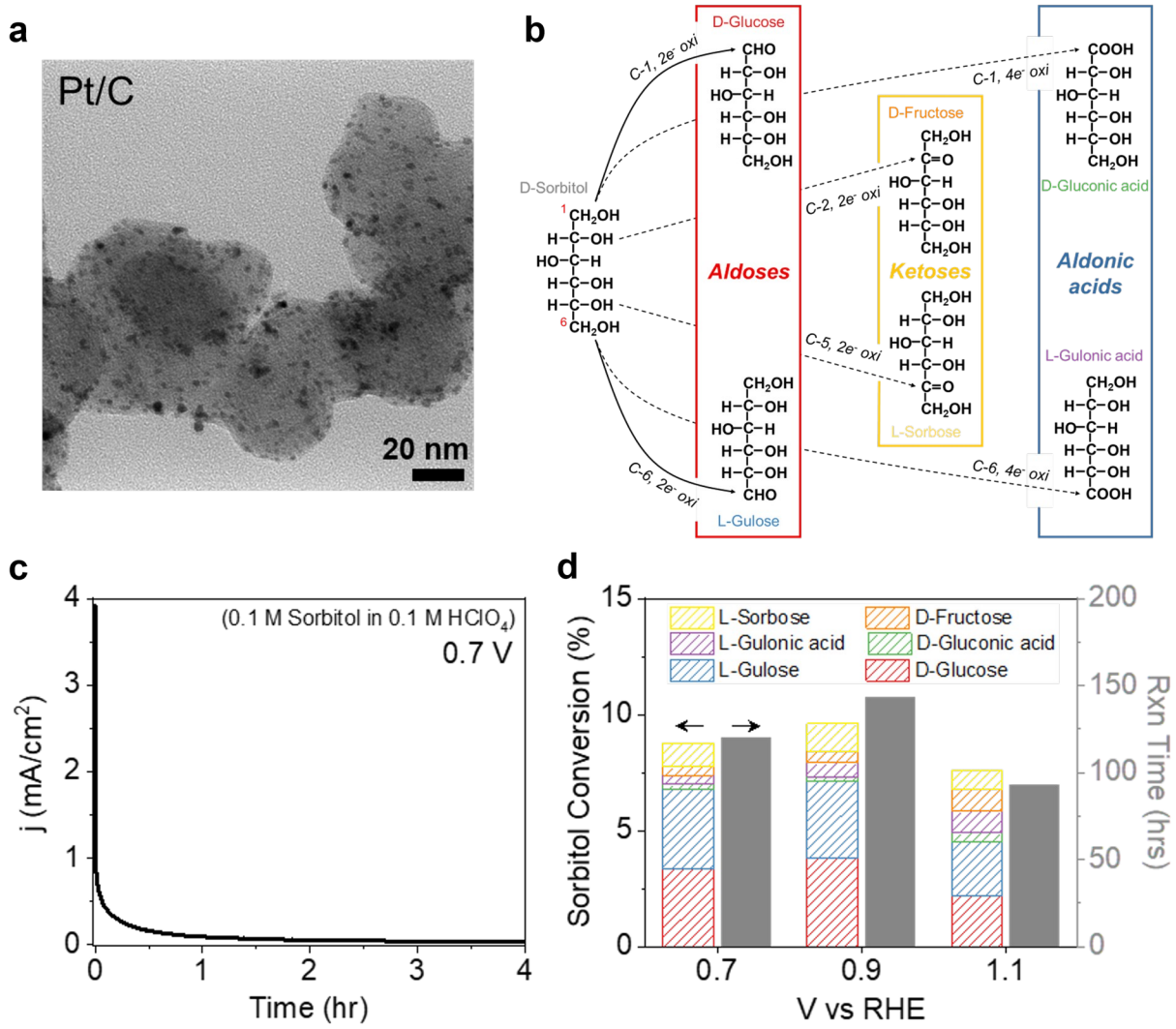

Figure 1. Electroconversion of sorbitol by Pt nanoparticles supported on C (Pt/C). (a) TEM image of Pt/C. (b) Electroconversion pathways to various products. The dominant pathways for Pt are the oxidation of terminal hydroxyls to aldehydes (solid lines) to form aldoses. (c) Steady-state current density exhibited by Pt/C at 0.7 V (vs. RHE). (d) Sorbitol conversion to various products (left y-axis) and the respective reaction times (right y-axis) under steady-state conditions at various potentials. All electrochemical measurements were conducted in a solution that was 0.1 M sorbitol and 0.1 M $HClO_4$ in water.

Sorbitol contains six hydroxyl groups. Depending on how the oxidation takes place, it can lead to three different product groups that are the aldoses, ketoses, and aldonic acids (Fig. 1b). These products were analyzed using high-pressure liquid chromatography-mass spectrometry (HPLC-MS) and calibration standards (Supplementary Fig. 4). Figure 1c shows that the steady-state current density for Pt/C biased at 0.7 V in 0.1 M sorbitol solution rapidly declines to <100 $\mu A/cm^2$. Similarly low activities were observed for other potentials beyond 0.7 V (Supplementary Fig. 5). Such low activity makes continuous, steady-state oxidation of sorbitol by Pt nanoparticles challenging in aqueous solutions at room temperature and ambient conditions.[17,30] It took an average of ~120 h to reach a sorbitol conversion of ~8 % (Fig. 1d). The sum of faradaic efficiencies closely matched the charge passed at the Pt/C electrode without any gas products detected (*e.g.* CO_2, Supplementary Fig. 6). Aldoses were the main product (60 – 80%), as expected from known platinum's catalytic behavior to oxidize primary alcohols and the more favorable conversion of terminal functional groups (Fig. 1d and Supplementary Fig. 6).[16,17,31] At applied potential >1.1 V, the overall behavior of activity/selectivity did not change but CO_2 and formic acid appeared as byproducts (Supplementary Fig. 7). In short, Pt nanoparticles can oxidize sorbitol majorly to aldoses at a very low activity under steady-state applied potentials.

To overcome the limitation of steady-state (SS) conversion, we sought to exploit the high transient activity of Pt nanoparticles only observed at the early periods within few seconds (Fig. 1c and Supplementary Fig. 5). Thus, instead of applying a constant fixed potential, we approached in a way so-called electrochemical potential cycling (EPC) that continuously scans the potential in the range 0.02 - 1.1 V at a scan rate of 100 mV/s (Fig. 2a). EPC allowed sorbitol oxidation to continue at high current densities of a few mA/cm^2 during the positive scan by the

oxidative potentials applied transiently throughout. Supplementary Figs. 8 and 9 show examples with and without sorbitol, respectively. While sorbitol oxidation occurs above 0.4 V, the largest contribution is from potentials greater than 0.75 V (Supplementary Fig. 8c). With a total of 4000 cycles applied, sorbitol oxidation proceeded at much faster rates compared to the SS conversion (Fig. 2a and Supplementary Fig. 8f). Conversion of ~10% was achieved at only a fraction of the time needed for SS runs (Fig. 2b). Furthermore, an unexpected improvement in ketoses selectivity was observed. Ketoses-to-aldoses ratio (K/A) increased over 6-fold from 0.26 (SS) to 1.67 (EPC) (Fig. 2c and Supplementary Fig. 10). Ketoses are produced by the oxidation of secondary hydroxyl groups as opposed to the oxidation of primary hydroxyl groups that lead to aldoses, and are less likely to form because of steric hindrance and lower reactivity of the former against the latter. Turnover frequency (TOF) was enhanced for all compounds by an order of magnitude between EPC and SS, and particularly for ketoses (~40-fold) (Fig. 2d). Thus, we found that EPC not only significantly improved intrinsic catalytic rates but also shifted selectivity toward products known to be difficult to form using Pt by conventional SS approaches.[16,17,31]

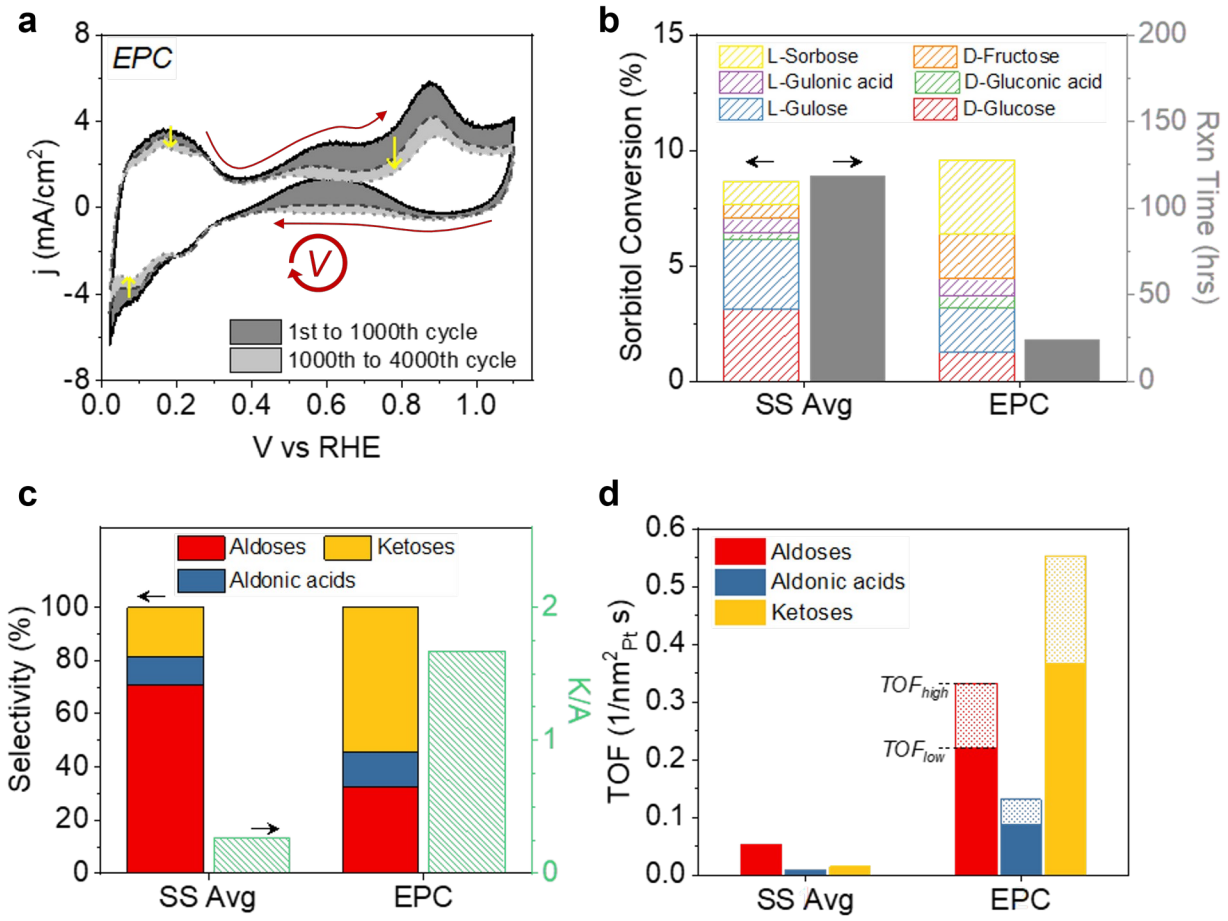

Figure 2. Electrochemical potential cycling (EPC) for sorbitol conversion. (a) Current density traces of EPC with a total of 4000 cycles at 100 mV/s. Red arrows indicate the scan direction. Yellow arrows indicate the trend of current density curves throughout. (b) Sorbitol conversion to various products and the reaction time of EPC compared against those of the average of SS runs at 0.7, 0.9, and 1.1 V. (c) Product selectivity and ketoses-to-aldoses ratio (K/A) by EPC and the average of SS runs. (d) Comparison of TOFs. TOF_{high} and TOF_{low} of EPC are estimated based on the average rate of the initial and final 50 cycles, respectively. Furthermore, the change of NP size from the initial (1.8 nm) to final (3.0 nm) state is considered which reduces the available Pt

surface area (estimated by hydrogen underpotential deposition) at the final state (Supplementary Fig. 12).

Throughout EPC, a gradual decline in the rate of sorbitol conversion was observed with an increasing number of cycles (Fig. 2a). Since EPC operates below 1.1 V, dissolution of Pt NPs was not the cause as measured by ICP-OES (Supplementary Fig. 11).[32,33] Nanoparticle coalescence and growth are observed during EPC as indicated by the loss in the Pt surface area and increase in particle size of 1.2 nm (Fig. 2a and Supplementary Fig. 12). However, it seems only minorly responsible for the rate decrease. As shown in Supplementary Fig. 13, replacing the used Pt/C electrode after 1400 cycles with a new Pt/C electrode did not fully recover the initial rate observed. Such observations suggest that the gradual decrease in rate may be due to the loss of sorbitol as a reagent and the accumulation of products. Indeed, we find a similar drop when sorbitol is partially replaced with products (Supplementary Fig. 14). Therefore, the rate decline during EPC seems intrinsic to the reaction and not a result of the method itself. In addition, taking into account the change in the Pt surface area, the TOF based on the last 50 cycles (TOF_{low}) was 70% of the initial TOF based on the first 50 cycles (TOF_{high}, Fig. 2d).

The key feature of EPC is its high activity in contrast to that of SS conversion (Fig. 2d). The initial activity measured at the onset of SS conversion, despite matching closely with EPC, does not persist and is lost as a steep decay (Supplementary Fig. 5). The SS conversion was conducted to avoid non-faradaic capacitive current contributions. Such short-lived activity may be related to charge transfer processes limited to pre-adsorbed species. However, the average charge

passed per cycle from sorbitol oxidation during EPC (14.3 mC/cycle) requires pre-adsorbed sorbitol molecules in a number equivalent to that of adsorbed H at ~106% coverage of Pt nanoparticles. This is physically not possible considering the size difference between H and sorbitol. In addition, the majority of the Pt surface is still available for hydrogen underpotential deposition during EPC (Fig. 2a). Lastly, application of staircase voltammetry confirmed that the high activity during EPC did not originate from surface-limited reactions due to pre-adsorbed species (see Supplementary text and Supplementary Figs. 15 - 17).

Depletion of sorbitol near the electrode as the cause of the fast activity decay during SS conversion could be ruled out as well. First, the time-dependent current density at various potentials exhibited a trend that does not match with diffusion-controlled currents (Supplementary Fig. 18). Moreover, convection induced to the electrolyte solution did not mitigate the loss of the high activity (Supplementary Fig. 19).

We suggest that oxidation/dehydrogenation of water by Pt leading to its surface oxidation is the main cause of the activity loss under SS conditions. Under positive potentials, the oxidative power of Pt can be applied to oxidizing water molecules leading to surface oxidation (O_{ads} or PtO_x) (Supplementary Fig. 20).[34–36] Tracing Pt NP surface oxidation in a sorbitol-free environment shows how it progresses at various fixed potentials (Fig. 3a). A common feature is that the oxidative power of Pt is rapidly lost: the rate of surface oxidation quickly levels off (Fig. 3a). It is expected that as Pt surface oxidation progresses toward equilibrium states determined for each potential, its capacity to oxidize water (or hydroxyls) will diminish. Its fast progression is what causes the rapid loss of high oxidative activity for sorbitol as well. Accordingly, when the Pt

NPs have lost their oxidative power through surface oxidation in a sorbitol-free 0.1 M $HClO_4$ under constant potential, injecting a small aliquot of concentrated sorbitol only resulted in minor activities for sorbitol oxidation (Fig. 3b and Supplementary Fig. 21).

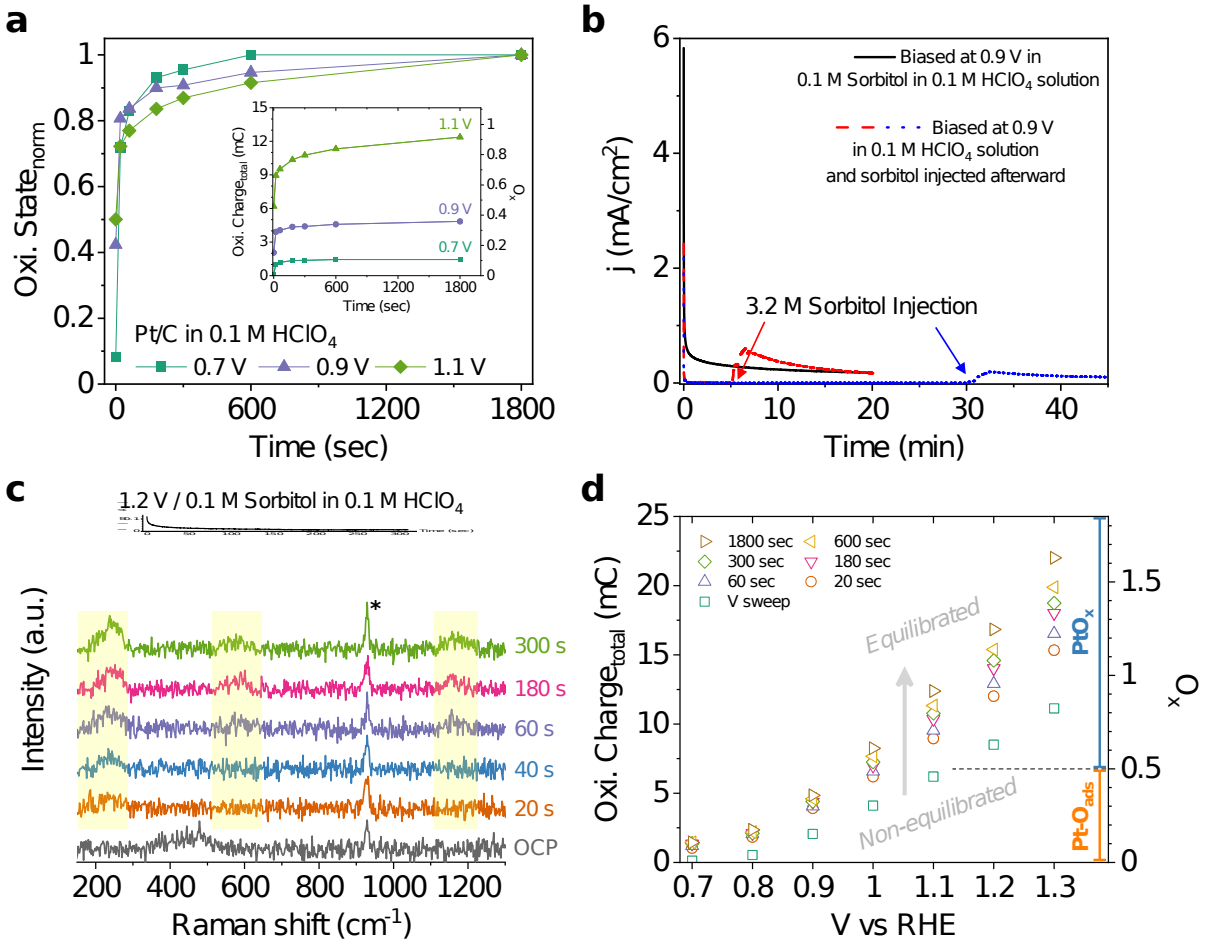

Figure 3. Surface oxidation of Pt and its relation to sorbitol conversion. (a) The relative degree of oxidation normalized by the final state reached at 1800 seconds for Pt/C in 0.1 M $HClO_4$ at various potentials. Inset shows the total charge passed and the associated oxygen atom per available surface Pt atom equivalent (O_x) for Pt/C surface oxidation. The initial points are the states reached by the potential sweep (at 100 mV/s) to each potential. (b) Sorbitol oxidation by a

pre-biased Pt/C in a sorbitol-free 0.1 M $HClO_4$. Pt/C is initially biased at 0.9 V in a pure 0.1 M $HClO_4$ solution (20 ml) and 3.2 M sorbitol solution (625µl in 0.1 M $HClO_4$) is injected near the Pt/C electrode under vigorous stirring to result in a ~ 0.1 M sorbitol solution (red dashed and blue dotted). The black solid curve is the original current density exhibited by Pt/C at 0.9 V in 0.1 M sorbitol in 0.1 M $HClO_4$. (c) SHINERS of polycrystalline Pt in 0.1 M sorbitol in 0.1 M $HClO_4$ solution at open circuit potential (OCP) and during steady-state conversion at 1.2 V. Inset shows the current measured at 1.2 V during spectra collection. Asterisk represents the perchlorate band (929 cm^{-1}) from the electrolyte. Each spectrum was collected for 10 seconds. (d) The extent of Pt/C surface oxidation measured by the total oxidation charge and the associated oxygen atom per available surface Pt atom equivalent (O_x) across various potentials for different periods in 0.1 M $HClO_4$. The studied periods range from the states reached by the potential sweep (at 100 mV/s) up to holding the bias for 1800 seconds. Before the place-exchange and formation of surface oxide PtO_x, O_{ads} can reach close to 0.5 in coverage as discussed in previous works.[34,35]

To further corroborate these observations, Raman spectroscopy was used to confirm the surface oxidation occurring under SS conversion of sorbitol. Shell-isolated nanoparticle-enhanced Raman spectroscopy (SHINERS) was applied by depositing silica-coated gold nanoparticles onto polycrystalline Pt used for spectroelectrochemistry (Supplementary Fig. 22).[37,38] Figure 3c shows the Raman spectra measured at open circuit potential and various times during SS conversion at 1.2 V. At open circuit, the $*CO_{ads}$ bands from the dissociative adsorption of sorbitol were observed at 374 (bridge) and 478 (atop) cm^{-1} which disappeared at positive

potentials (Supplementary Fig. 3). When biased at 1.2 V, new bands appeared around 240, 580, and 1160 cm^{-1} that coincided with the decay of sorbitol conversion current (Fig. 3c inset). The same bands appeared when biased at 1.2 V without sorbitol present in solution and can be assigned to the surface oxides PtO_x formed above 1.1 V (Supplementary Fig. 23).[38] As shown in Fig. 3d, surface oxidation charge analysis of Pt/C in 0.1 M $HClO_4$ also indicates the formation PtO_x at potentials greater than 1.1 V (Supplementary Fig. 24). Above 1.1 V, place-exchange is known to occur thus converting Pt-O_{ads} to a surface oxide PtO_x.[34–36] At SS conversions below 1.1 V, loss of oxidative activity is expected as well as the Pt surface oxidizes to form an equilibrium coverage O_{ads} (Fig. 3d and Supplementary Fig. 25). Therefore, the loss of oxidative power following Pt surface oxidation toward equilibrium states causes the fast decay of sorbitol oxidation activity at each potential. Leveraging this knowledge, EPC focuses on the high oxidative power of the non-equilibrated Pt/water interface through the continuous cycling of potential involving a positive potential sweep for electrooxidation and a quick reversal to reduce the surface back to pristine Pt before reaching equilibrium.

It should be noted that restoration of the metallic Pt surface is evident from the overlapping hydrogen underpotential deposition region during consecutive cycles (Supplementary Fig. 8b). The gradual decline of hydrogen underpotential deposition current observed in the long term is due to particle coalescence and loss of total surface area as mentioned above (Fig. 2a and Supplementary Fig. 12). Moreover, it is speculated that Pt may be less oxidized than the non-equilibrated states reached during the potential sweep in a sorbitol-free condition as can be deduced from the behavior of Pd, a Pt-group element (Supplementary Fig. 26).

Previous work suggests that the first step of sorbitol oxidation is a proton-electron transfer from the hydroxyl group to form an oxygen-bound intermediate state.[39] The following proton-electron transfer from the alpha carbon ultimately generates a carbonyl. Tafel analysis of EPC suggests that the second step is rate-limiting (Supplementary Fig. 27).[40] Thus, the non-equilibrated Pt surfaces can readily oxidize the hydroxyl group in the first step which may be expected from their capacity to strongly bind oxygen atoms. However, such capacity is lost at fixed potentials with Pt surfaces close to oxidation equilibrium leading to a significant loss of catalytic activity.

Besides the order of magnitude improvement in TOF, EPC also exhibits an increase in the ketoses production (Fig. 2). This observation is unexpected considering the selectivity observed from SS conversions as well as how Pt has been regarded as an electrocatalyst that is limited to oxidation of only terminal hydroxyl groups.[17,31] Here, we demonstrate that a non-equilibrated Pt surface with a high oxidative capacity is however active for secondary alcohol oxidation. Figure 4 shows EPC applied to various polyols such as glycerol (C_3), erythritol (C_4), and ribitol (C_5). TOFs are improved by one (for aldoses) to two (for ketoses) orders of magnitude across all polyols (Supplementary Figs. 28 – 30). In particular, the enhanced ketoses formation raises the K/A by 3 to 5-fold when comparing against that of SS conversion. This result clearly suggests that there is an underutilized capacity of Pt for electrooxidation of organic compounds and the often-considered low catalytic activity of Pt is due to equilibration of its surface through surface oxidation under prolonged steady-state conditions rather than intrinsic inactivity.

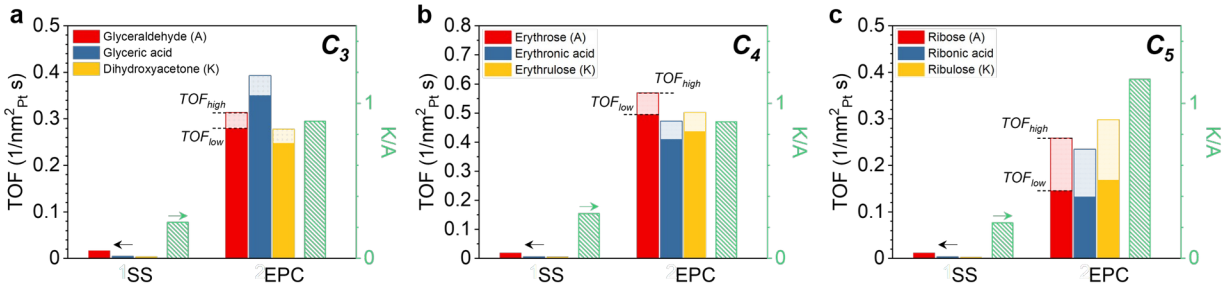

Figure 4. Application of EPC to polyols other than sorbitol. TOFs and K/A for both SS conversion (at 0.9 V) and EPC applied to (a) glycerol (C_3 polyol), (b) erythritol (C_4 polyol), and (c) ribitol (C_5 polyol). TOF_{high} and TOF_{low} of EPC are estimated based on the average rate of the initial and final 50 cycles, respectively. Furthermore, the change in the available Pt surface area (estimated by hydrogen underpotential deposition) as a result of NP growth (Supplementary Fig. 12) at the final state is considered.

Application of the non-equilibrated Pt surface for electrooxidation could be achieved analogously through short potential pulses. By the repetitive potential application between 0.02 and 1.0 V for short periods, high-rate sorbitol conversion and enhanced ketoses formation (i.e., high K/A) were observed (Supplementary Fig. 31). Moreover, it was confirmed that the small amount of $*CO_{ads}$ generated by the dissociative adsorption of sorbitol during EPC (Supplementary Fig. 3) do not play a major role in the reactivity of Pt NPs. During potential pulsing, there was a negligible formation of $*CO_{ads}$ despite similar activity for sorbitol oxidation (Supplementary Fig. 31).

Shifting the positive end of EPC above 1.1 V allows access to the non-equilibrated

surface oxide PtO_x beyond the metallic Pt with low coverage of O_{ads} (Fig. 3d).[34–36] Its presence is connected to another high current density regime as shown in Supplementary Fig. 32. Furthermore, the PtO_x is reduced far below the potential range it is formed and thus, becomes a metastable oxide during the reverse potential scan (Supplementary Fig. 20). The greater presence of such metastable PtO_x also induces a strong oxidative activity for sorbitol (Supplementary Fig. 32).

As expected with non-equilibrated surfaces, EPC applied to sorbitol oxidation with the positive end at 1.3 V exhibited high TOFs (Supplementary Fig. 33). Meanwhile, aldoses selectivity increased with a K/A of 0.6. In comparison against the original EPC applied to 1.1 V, selectivity shift could be correlated with the presence of the non-equilibrated PtO_x during the forward scan (> 1.1 V) and the reverse as a metastable oxide (Supplementary Fig. 33). Therefore, selectivity seems to be dictated by the non-equilibrium surface phase present during potential cycling. It is speculated that a metallic Pt surface allows sorbitol adsorption in a configuration such that inner hydroxyl groups become more accessible to its surface. Further study is needed regarding the sensitivity to the surface phase present under non-equilibrium conditions.

To make use of a catalyst or method in an applicable setting, it needs to be transferable to an electrolyzer in a 2-electrode configuration. Application of continuous alteration of potentials to electrolyzers is nontrivial since they typically operate under a static voltage difference between the two electrodes (Supplementary Fig. 34). Therefore, despite the benefits of potential pulse applications, previous works have only focused on what occurs on the working electrode in a 3-electrode configuration.[18–24] Doing so with the EPC approach required a certain strategy to be

devised.

The need for a constant potential shift on one electrode places a constraint on the other: the second electrode has to simultaneously shift its potential since the voltage applied is referenced to each other (see Supplementary text and Supplementary Fig. 35). Thus, careful consideration of the other electrode in terms of its reactions under potential alteration, the potential range required, and how both electrodes operate in a synchronized fashion is necessary for an electrolyzer to operate based on the principles of EPC. We propose a symmetric single compartment (SSC) system, in which both electrodes are identical and perform the same set of reactions in one compartment. Its example operation in a pure electrolyte solution demonstrated both electrodes to behave in a controlled manner under potential alterations (see Supplementary text and Supplementary Fig. 36). Then, voltage cycling (VC), the 2-electrode equivalent to the 3-electrode EPC, can be successfully applied to the device (Supplementary Fig. 37). The same procedures were followed to test an electrolyte solution containing sorbitol which proved the applicability of VC to sorbitol electrooxidation together with the coupled half-reaction of water reduction to H_2 gas (see Supplementary text and Supplementary Figs. 38 and 39).

The schematic of the device to utilize VC for sorbitol conversion is shown in Fig. 5a. Two identical Pt/C electrodes alternate between sorbitol oxidation and H_2 production, a valuable co-product. The necessary conditions for VC to mimic EPC were confirmed as a continuous voltage scan in between ±1.4 V (Supplementary Fig. 40). Fig. 5b shows the current density curves as a result. The positive scan (red) oxidized sorbitol on one electrode while H_2 was produced at the other electrode. The same occurred on the negative scan (blue) with the potential signs and

the roles of the two electrodes switched. The absolute scan width |V| in both directions was dynamically reduced during VC to accommodate changes in the IR loss from the steadily declining current density (Supplementary Fig. 41).

Production of H_2 was confirmed and measured throughout (Fig. 5c). The overall charge balance in the system was approximately closed considering that the amount of reductive charge used for H_2 production was very close to the sum of oxidative charges required to form carbon-containing products in the liquid phase or as CO_2 (Fig. 5d). Over 20 % of sorbitol conversion to products was demonstrated by VC (Fig. 5e). It also exhibited a rate order-of-magnitude higher compared to a typical operation under static voltage application (Supplementary Fig. 42). In addition, undesirable humin formation occurred under the static voltage condition, representing an additional issue for its application toward sorbitol electroconversion. In contrast, VC did not show signs of humin production (Supplementary Figs. 42 and 43). VC was also able to promote ketoses formation as demonstrated with EPC (Fig. 5f).

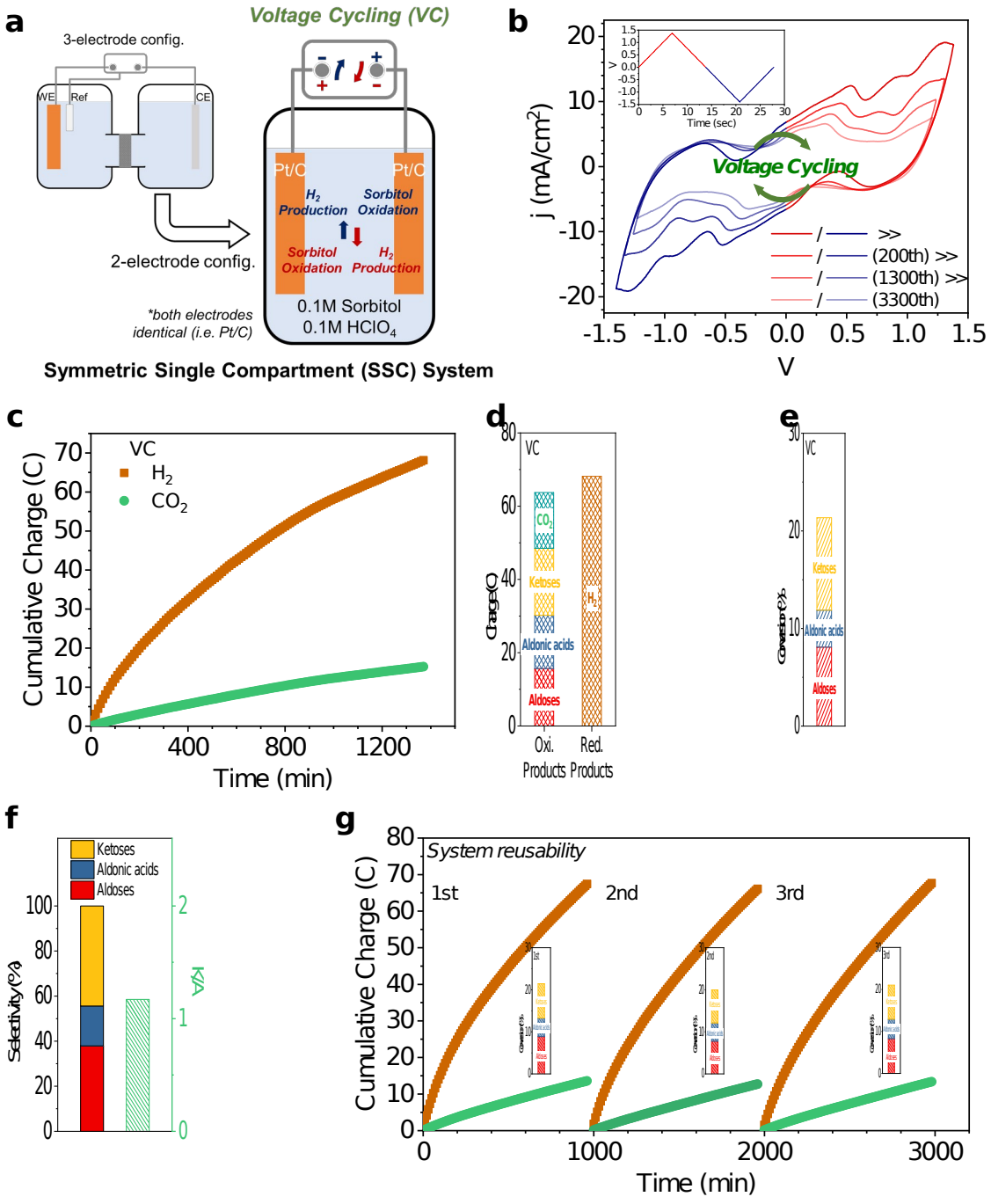

Figure 5. Voltage Cycling (VC) for sorbitol conversion. (a) A schematic of the SSC device used and its operation under VC. It contains two identical Pt/C electrodes of 1 cm^2 geometric area at a loading 120 $\mu g_{Pt}/cm^2$ and the electrolyte is 0.1 M sorbitol in 0.1 M $HClO_4$. (b) VC applied at 200 mV/s for a total of 3300 cycles. The inset shows a single voltage scan that is applied repetitively.

(c) Time-dependent cumulative charge equivalents for H_2 (2-electron reduction) and CO_2 (2-electron oxidation) produced by VC. (d) The total charge equivalents for oxidation and reduction products. Sorbitol conversion to various products (e) and selectivity and K/A (f) by VC. (g) Repeated uses of the same SSC device for sorbitol conversion by VC.

We tested the reusability of the system by replacing the sorbitol-containing electrolyte post-reaction with a fresh solution and applying VC for multiple rounds. The tests resulted in production rates mostly unaltered for at least three consecutive cycles (Fig. 5g and Supplementary Fig. 44). It is because not only VC operates at potentials where Pt NP dissolution is negligible (Supplementary Fig. 11), but also because NP coalescence and growth mostly occur at the smallest initial size and slows down as particles grow (Supplementary Fig. 45). Furthermore, nanoparticle size in the range of 2 to 5 nm does not seem to critically affect the catalytic behavior under these conditions.

Through the adoption of a novel electrochemical approach, while using standard Pt nanoparticles as catalysts, we have demonstrated high-rate polyol electrolysis coupled with H_2 production. The fundamentals of the method are anticipated to be applicable to various feedstocks and biomass-derived compounds for electrochemical conversion. Moreover, by taking advantage of the latest advances in nanoscience, such as imposing certain structural characteristics (*e.g.*, morphology and composition) to nanoparticles closely linked to their catalytic behavior (*e.g.*, adsorption strength and durability), the approach demonstrated here has much room for further development.

Methods

Pt/C working electrode preparation for a three-electrode configuration

Pt/C (Premetek, 20% Pt on Vulcan) is dispersed in ethanol (0.4 mg_{Pt}/ml) by sonication. The homogeneous Pt/C solution is drop-casted onto a 1 cm^2 carbon paper support (Sigracet) at a loading of 40 $\mu g_{Pt}/cm^2$ and dried under ambient conditions over 24 hours.

Electrochemical experiments in a three-electrode configuration

All measurements are conducted in a H-cell with the two compartments separated by a Nafion membrane (Supplementary Fig. 2). Pt/C loaded on carbon paper (40 $\mu g_{Pt}/cm^2$, 1 cm^2_{geo}) is used as a working electrode (Pt area estimated by H-UPD is 32.2 cm^2_{Pt}). Reversible hydrogen electrode (RHE) is used as a reference electrode, while a platinum wire is used as a counter electrode. The working compartment contains 0.1 M sorbitol (Sigma Aldrich, 99%) in a 0.1 M $HClO_4$ solution and the counter compartment only contains 0.1 M $HClO_4$. For direct comparisons, tests are also conducted with the working compartment containing only 0.1 M $HClO_4$ (without sorbitol). The working compartment is sparged with Ar gas before the start of any electrochemical measurement for > 15 min and the Ar purge (20 sccm) continues throughout the measurement. The working compartment is stirred using a magnetic stir bar.

Voltammetry sweeps (linear sweep voltammetry and cyclic voltammetry) are conducted at a scan rate of 100 mV/s, unless stated otherwise. Chronoamperometry tests are conducted following a few CVs in the range of 0.02 - 1.3 V till stabilization and ending the scan at the selected potential of interest to continue into steady-state current measurement right afterwards (*e.g.*, CV ending at

0.7 V before continuing CA at 0.7 V). This eliminates current contributions from the rapidly decaying non-faradaic capacitive current that is proportional to ΔV (= V_2(applied) - V_1(prior)) at early periods of CA. For all measurements in this three-electrode configuration, 85% of the ohmic loss (typical solution resistance ~10 Ohm) is compensated by the potentiostat (Biologic) in real-time.

For experiments that involve product analysis, faradaic efficiency (FE, %) is estimated by the amount of charge needed to produce each product i ($Q_{product,i}$) divided by the total charge (Q_{total}) passed.

$$FE(\%)\ of\ product\ i = 100 \times \frac{Q_{product,i}}{Q_{total}} = 100 \times \frac{n_{e,product\ i} \times C \times N_{product,i}}{Q_{total}}$$

$$C: Faraday\ constant\ 96{,}485 \frac{C}{mol},\ N_{product,i}: mols\ of\ product\ i$$

Conversion (%) to each product is estimated as follows,

$$Conversion\ product\ i\ (\%) = 100 \times \frac{M_{product,i}}{M_{sorbitol}} \left(M_{product,i}: conc.\ of\ product\ i,\ M_{sorbitol} = 0.1\ M\right)$$

Selectivity (%) to each product group is estimated as follows,

$$Selectivity(\%) = 100 \times M_{product} / M_{total} \left(M_{product}: M_{aldoses} \vee M_{aldonic\ acids} \vee M_{ketoses},\ M_{total} = \sum M_{product}\right)$$

Turnover frequency (TOF) is estimated as follows,

$$TOF_{product} = \frac{N_A \times N_{product}}{Area_{Pt} \times total\ reaction\ time}$$

$$\left(N_A: Avogadro\ constant,\ N_{product}: mols\ of\ product,\ Area_{Pt}: Pt\ area\ estimated\ by\ H\ UPD,\ 3.22 \times 10^{15}\ nm^2_{Pt}\right)$$

*$Area_{Pt}$ remains the same for steady-state runs confirmed by H-UPD

Electrochemical Potential Cycling (EPC)

A standard EPC run is conducted in the identical three-electrode H-cell configuration (Supplementary Fig. 2). It is performed by scanning the potential of the Pt/C working electrode in between 0.02 and 1.1 V at 100 mV/s. A single cycle is a complete potential scan that consists of both the positive sweep from 0.02 to 1.1 V and the negative sweep back to 0.02 V. A total of 4000 cycles is performed with the products in liquid phase analyzed by HPLC-MS and the gas product (*i.e.*, CO_2) measured at the outlet in regular intervals by GC. TOF_{high} and TOF_{low} are calculated by estimating $N_{product}$ of the first and last 50 cycles, respectively, based on the amount of charge passed for each compared against the total charge passed and considering the total amount of products detected. While TOF_{high} is based on the initial area of Pt NPs, TOF_{low} takes into account the growth of particles during EPC (Supplementary Fig. 12) and their final area being 0.66 of the initial area estimated by H-UPD. This relative change in the area matches closely with the estimate based on avg. particle size increase (approx. 40% loss of initial area). As TOF represents intrinsic activity, the amount of time spent in between 0.02 - 0.35 V in the H-UPD region during EPC is not considered as part of the reaction time for TOF estimation purposes only (otherwise, Rxn time plotted in figures such as Fig. 2b is the actual total time spent for the entire EPC run).

Product Analysis

Sorbitol oxidation products dissolved in the liquid phase (electrolyte solution) are analyzed by high pressure liquid chromatography - mass spectrometry (HPLC-MS) instrumentation (Waters).

The HPLC system runs using a binary gradient pump and an autosampler with a 20 µl sample loop. Since the products are not suited for UV-vis absorption (*i.e.*, their major functionality being hydroxides) or refractive index detection (*i.e.*, too low of concentration below the detection limit of RID), a MS (Electrospray ionization with Single Quadrupole mass detection) is used for their analysis. Product separation is carried out in a LC column (XBridge BEH Amide XP 2.5 µm, 3 mm X 150 mm) and the mobile phase is LC-MS grade 90% acetonitrile/10% water with 0.08% NH_4OH (v/v/v) at a flow rate of 1 ml/min. The MS operates in ES- mode with capillary voltage 2.8 kV, cone voltage 25 V, source temperature 120 ºC, desolvation temperature 350 ºC, desolvation gas flow 550 L/hr, and cone gas flow 50 L/hr. Sample injection volume is 20 µl and each sample is prepared by diluting the original solution (*i.e.*, standard analytes and electrolysis reaction solutions) by a factor of 1/125 in a LC-MS grade 75% acetonitrile/25% water (v/v). The calibration standards of known concentrations are prepared in the same electrolyte (*i.e.*, 0.1 M $HClO_4$) solution and are regularly tested each day before sample testing to ensure that sensitivity factors are accurate.

For electrolysis runs that require detection and quantification of CO_2 and H_2 gas, the gas outlet is connected to a gas chromatograph (Buck Scientific) equipped with a thermal conductivity detector (TCD) and flame ionization detector (FID) to sample gaseous products. They are separated by HayeSep D and Molsieve 5A columns under Ar as a carrier gas and at a temperature of 45 ºC. H_2 gas is measured by the TCD and CO_2 passes through a methanizer tube before being detected by the FID.

Surface oxidation analysis of Pt/C

Pt/C loaded on carbon paper is used as a working electrode in a H-cell filled with 0.1 M $HClO_4$. Reversible hydrogen electrode (RHE) is used as a reference electrode and the working compartment is constantly purged with Ar gas at 20 sccm. Surface oxidation charge during the potential sweep (at 100 mV/s) to each potential is estimated by integrating the charge under the surface oxidation curve in the voltammogram ($\geq$ 0.7 V) with the double-layer charging current as the baseline (Supplementary Fig. 20a). Surface oxidation charge at different times for each potential is estimated by following the identical procedure as the chronoamperometry tests for sorbitol conversion: the potential sweep to the selected potential is immediately followed by a fixed potential application for different time periods (*e.g.*, CV ending at 0.7 V and then, continuing CA at 0.7 V). At the end of each period, a reverse potential sweep to the H-UPD region is conducted to reduce the Pt surface with prolonged times for surface oxidation resulting in a larger total charge for reduction (Supplementary Fig. 20b). The additional reduction charge measured by comparing against the reverse potential sweep without the fixed potential application is added to the surface oxidation charge during the potential sweep (V sweep) to estimate the total oxidation charge as a function of time and potential. The oxygen atom per available surface Pt atom equivalent (O_x) is estimated by dividing the total oxidation charge to the twice the amount of the H-UPD charge (6.755 mC) assuming 1-to-1 correlation of the underpotential deposited H and the surface Pt atom.

In situ Electrochemical Raman Spectroscopy

The silica-coated gold nanoparticles ($Au@SiO_2$) were prepared following the Frens' method to prepare the gold nanoparticles and coating a thin layer of silica.[37,38,41] In short, a gold nanoparticle (55 nm size) solution was prepared by injecting 1 wt.% sodium citrate solution into a boiling 0.01 wt.% $HAuCl_4$ solution. Then, 30 ml of the gold nanoparticle solution was first injected with 0.4 ml APTMS (3-aminopropyltrimethoxysilane) (1mM) and stirred for 15 min at room temperature. 3.2 ml sodium silicate solution (0.54 wt.%, pH 10.2 – 10.3) was added and stirred for 3 min. The solution was transferred to a water bath (90 ˚C) and stirred for 20 min. Afterward, the solution was cooled down in an ice bath and centrifuged at 5500 rpm for 15 min for washing and redispersion.

$Au@SiO_2$ were deposited on a polycrystalline Pt wire electrode and dried under vacuum. $Au@SiO_2$ deposited Pt electrode was cleaned by applying -2.0 V vs Ag/AgCl in a neutral electrolyte solution multiple times.[42] Then, it was transferred to a spectroelectrochemical cell filled with Ar purged 0.1 M $HClO_4$ or 0.1 M Sorbitol in 0.1 M $HClO_4$. Raman spectra were recorded with Xplora Plus confocal Raman microscope (HORIBA) using a He–Ne laser with a wavelength of 637.8 nm. The spectrometer was calibrated using a Si wafer. Each spectrum was collected for 10 seconds.

Voltage Cycling (VC) in a Symmetric Single Compartment (SSC) system

The SSC device consists of two identical Pt/C (120 $\mu g_{Pt}/cm^2$, 1 cm^2_{geo}) electrodes facing each other in a single compartment that contains a 10 ml solution of 0.1 M sorbitol in 0.1 M $HClO_4$. Both electrodes are prepared from a solution of Pt/C (Premetek, 20% Pt on Vulcan) dispersed in

ethanol (0.4 mg_{Pt}/ml) by sonication. The compartment is constantly purged with Ar (10 sccm) and the gas outlet is connected to a GC. For preliminary testing of the device in a 3-electrode configuration (Supplementary Fig. 40), a reversible hydrogen electrode (RHE) is used as a reference and placed at the center between the two Pt/C electrodes. Otherwise, in a 2-electrode configuration, the voltage (V) applied is the applied bias between the two electrodes. The resistance between the reference and either Pt/C electrode is approximately 10 Ohm (the total resistance between the two Pt/C electrodes is ~ 20 Ohm). Voltage is scanned at 200 mV/s in between +1.4 V and -1.4 V and throughout a total of 3300 cycles, the positive and negative end of V applied is reduced (final voltage ±1.22 V) to accommodate changes in the V_{IR} (Supplementary Fig. 41).

References

1. Bendixen, F. B. *et al.* Industrial Hydrogen Production. *Science (80-.).* **759**, 756–759 (2019).

2. De Luna, P. *et al.* What would it take for renewably powered electrosynthesis to displace petrochemical processes? *Science (80-.).* **364**, (2019).

3. Chu, S., Cui, Y. & Liu, N. The path towards sustainable energy. *Nat. Mater.* **16**, 16–22 (2016).

4. Service, R. F. Renewable bonds. *Science (80-.).* **365**, 1236–1239 (2019).

5. Schiffer, Z. J. & Manthiram, K. Electrification and Decarbonization of the Chemical Industry. *Joule* **1**, 10–14 (2017).

6. Cha, H. G. & Choi, K. S. Combined biomass valorization and hydrogen production in a photoelectrochemical cell. *Nat. Chem.* **7**, 328–333 (2015).

7. You, B., Liu, X., Jiang, N. & Sun, Y. A General Strategy for Decoupled Hydrogen Production from Water Splitting by Integrating Oxidative Biomass Valorization. *J. Am. Chem. Soc.* **138**, 13639–13646 (2016).

8. Li, T., Cao, Y., He, J. & Berlinguette, C. P. Electrolytic CO2 Reduction in Tandem with Oxidative Organic Chemistry. *ACS Cent. Sci.* **3**, 778–783 (2017).

9. Sherbo, R. S., Delima, R. S., Chiykowski, V. A., MacLeod, B. P. & Berlinguette, C. P. Complete electron economy by pairing electrolysis with hydrogenation. *Nat. Catal.* **1**, 501–507 (2018).

10. Kim, R. S. & Surendranath, Y. Electrochemical Reoxidation Enables Continuous Methane-to-Methanol Catalysis with Aqueous Pt Salts. *ACS Cent. Sci.* **5**, 1179–1186 (2019).

11. Liu, D. *et al.* Selective photoelectrochemical oxidation of glycerol to high value-added dihydroxyacetone. *Nat. Commun.* **10**, (2019).

12. Leow, W. R. *et al.* Chloride-mediated selective electrosynthesis of ethylene and propylene oxides at high current density. *Science (80-.).* **368**, 1228–1233 (2020).

13. She, Z. W. *et al.* Combining theory and experiment in electrocatalysis: Insights into materials design. *Science (80-.).* **355**, (2017).

14. Ross, M. B. *et al.* Designing materials for electrochemical carbon dioxide recycling. *Nat. Catal.* **2**, 648–658 (2019).

15. Kwon, Y., Birdja, Y., Spanos, I., Rodriguez, P. & Koper, M. T. M. M. Highly Selective Electro-Oxidation of Glycerol to Dihydroxyacetone on Platinum in the Presence of Bismuth. *ACS Catal.* **2**, 759–764 (2012).

16. Kimura, H., Tsuto, K., Wakisaka, T., Kazumi, Y. & Inaya, Y. Selective oxidation of glycerol on a platinum-bismuth catalyst. *Appl. Catal. A Gen.* **96**, 217–228 (1993).

17. Kwon, Y., de Jong, E., van der Waal, J. K. & Koper, M. T. M. Selective Electrocatalytic Oxidation of Sorbitol to Fructose and Sorbose. *ChemSusChem* **8**, 970–973 (2015).

18. Lee, C. W., Cho, N. H., Nam, K. T., Hwang, Y. J. & Min, B. K. Cyclic two-step electrolysis for stable electrochemical conversion of carbon dioxide to formate. *Nat. Commun.* **10**, 1–8 (2019).

19. Engelbrecht, A. *et al.* On the Electrochemical CO 2 Reduction at Copper Sheet Electrodes with Enhanced Long-Term Stability by Pulsed Electrolysis . *J. Electrochem. Soc.* **165**, J3059–J3068 (2018).

20. Arán-Ais, R. M., Scholten, F., Kunze, S., Rizo, R. & Roldan Cuenya, B. The role of in situ generated morphological motifs and Cu(i) species in C2+ product selectivity during CO2 pulsed electroreduction. *Nat. Energy* **5**, 317–325 (2020).

21. Gopeesingh, J. *et al.* Resonance-Promoted Formic Acid Oxidation via Dynamic Electrocatalytic Modulation. *ACS Catal.* **10**, 9932–9942 (2020).

22. Blanco, D. E., Lee, B. & Modestino, M. A. Optimizing organic electrosynthesis through controlled voltage dosing and artificial intelligence. *Proc. Natl. Acad. Sci.* **116**, 17683–17689 (2019).

23. Wattanakit, C., Yutthalekha, T., Asssavapanumat, S., Lapeyre, V. & Kuhn, A. Pulsed electroconversion for highly selective enantiomer synthesis. *Nat. Commun.* **8**, 1–8 (2017).

24. Sakaguchi, H., Matsumura, H. & Gong, H. Electrochemical epitaxial polymerization of single-molecular wires. *Nat. Mater.* **3**, 551–557 (2004).

25. Kobayashi, H. *et al.* Synthesis of sugar alcohols by hydrolytic hydrogenation of cellulose over supported metal catalysts. *Green Chem.* **13**, 326–333 (2011).

26. Bozell, J. J. & Petersen, G. R. Technology development for the production of biobased products from biorefinery carbohydrates—the US Department of Energy's "Top 10" revisited. *Green Chem.* **12**, 539 (2010).

27. Besson, M., Gallezot, P. & Pinel, C. Conversion of Biomass into Chemicals over Metal Catalysts. *Chem. Rev.* **114**, 1827–1870 (2014).

28. Zhang, Z. & Huber, G. W. Catalytic oxidation of carbohydrates into organic acids and furan chemicals. *Chem. Soc. Rev.* **47**, 1351–1390 (2018).

29. Proença, L. F. A. *et al.* On the oxidation of d-sorbitol on platinum single crystal electrodes: a voltammetric and in situ FTIRS study. *Electrochim. Acta* **44**, 735–743 (1998).

30. Proença, L. *et al.* Electrocatalytic oxidation of d-sorbitol on platinum in acid medium: analysis of the reaction products. *J. Electroanal. Chem.* **432**, 237–242 (1997).

31. Coutanceau, C., Baranton, S. & Kouamé, R. S. B. Selective Electrooxidation of Glycerol Into Value-Added Chemicals: A Short Overview. *Front. Chem.* **7**, 1–15 (2019).

32. Topalov, A. A. *et al.* Dissolution of Platinum: Limits for the Deployment of Electrochemical Energy Conversion? *Angew. Chemie Int. Ed.* **51**, 12613–12615 (2012).

33. Cherevko, S., Zeradjanin, A. R., Keeley, G. P. & Mayrhofer, K. J. J. A Comparative Study on Gold and Platinum Dissolution in Acidic and Alkaline Media. *J. Electrochem. Soc.* **161**, H822–H830 (2014).

34. Jerkiewicz, G., Vatankhah, G., Lessard, J., Soriaga, M. P. & Park, Y. S. Surface-oxide growth at platinum electrodes in aqueous H2SO 4 Reexamination of its mechanism through combined cyclic-voltammetry, electrochemical quartz-crystal nanobalance, and Auger electron spectroscopy measurements. *Electrochim. Acta* **49**, 1451–1459 (2004).

35. Sasaki, K., Marinkovic, N., Isaacs, H. S. & Adzic, R. R. Synchrotron-Based In Situ Characterization of Carbon-Supported Platinum and Platinum Monolayer Electrocatalysts. *ACS Catal.* **6**, 69–76 (2016).

36. Drnec, J. *et al.* Initial stages of Pt(111) electrooxidation: dynamic and structural studies by surface X-ray diffraction. *Electrochim. Acta* **224**, 220–227 (2017).

37. Li, J. F. *et al.* Surface analysis using shell-isolated nanoparticle-enhanced Raman spectroscopy. *Nat. Protoc.* **8**, 52–65 (2013).

38. Huang, Y. F., Kooyman, P. J. & Koper, M. T. M. M. Intermediate stages of electrochemical oxidation of single-crystalline platinum revealed by in situ Raman spectroscopy. *Nat. Commun.* **7**, 1–7 (2016).

39. Proença, L., Lopes, M. I. S. I. S., Fonseca, I., Hahn, F. & Lamy, C. An in situ IR reflectance spectroscopic study of the electro-oxidation of d-sorbitol on platinum. *Electrochim. Acta* **44**, 1423–1430 (1998).

40. Fang, Y. H. & Liu, Z. P. Tafel kinetics of electrocatalytic reactions: From experiment to first-principles. *ACS Catal.* **4**, 4364–4376 (2014).

41. FRENS, G. Controlled Nucleation for the Regulation of the Particle Size in Monodisperse Gold Suspensions. *Nat. Phys. Sci.* **241**, 20–22 (1973).

42. Li, J.-F., Rudnev, A., Fu, Y., Bodappa, N. & Wandlowski, T. In Situ SHINERS at Electrochemical Single-Crystal Electrode/Electrolyte Interfaces: Tuning Preparation Strategies and Selected Applications. *ACS Nano* **7**, 8940–8952 (2013).

Acknowledgments

This work was mostly based on seed funding from the Global Climate and Energy Program at Stanford University. Part of the work was supported by a research grant (9455) from VILLUM FONDEN. M.C. acknowledges additional support from a Sloan Fellowship. M.Z. acknowledges the support from the U.S. Department of Energy (DOE), Office of Science, Basic Energy Sciences, under Contract No. DE-AC02-05CH11231. The LBNL Catalysis Facility is supported by DOE under the same contract number. Part of this work was performed at the Stanford Nano Shared Facilities (SNSF), supported by the National Science Foundation under award ECCS-2026822.

Author contributions

D.K. designed and performed the experiments. D.K. conducted product analysis with assistance from C.S. and M.Z. M.C. supervised the project. D.K. and M.C. wrote the manuscript with comments from all authors.

Competing interests

The authors declare no competing interests

Correspondence and requests for materials should be addressed to M.C.

Data availability

The data that support the findings of this study are available from the corresponding author upon reasonable request.